# Active Semiconductor-Based Grating Waveguide Structures

Nirit Dudovich, Guy Levy-Yurista, Avner Sharon, Asher A. Friesem, *Fellow, IEEE*, and Hans-Georg Weber

***Abstract*—Under certain conditions, a high-finesse resonance phenomenon can occur in a grating waveguide structure (GWS). By varying these conditions, a shift in the resonance wavelength can be achieved. Specifically, utilizing the high finesse property of the GWS, small changes in the refractive index can result in a tuning range larger than the resonance bandwidth. Here, we consider different electric-field and charge carrier mechanisms that can affect the refractive index in semiconductor materials, and exploit them in order to control the refractive index change and, therefore, the resonance wavelength in the GWS. The predicted results are verified experimentally with an active GWS formed with semiconductor materials and operated in a reverse voltage configuration.**

***Index Terms*—Active filters, gratings, resonance, semiconductor devices, tunable filters, tuning, waveguides.**

## I. Introduction

ALTHOUGH diffraction of light from periodic structures has been investigated for many years, recent developments in electron beam and lithographic technologies have led to a resurgence of research in this field. This is particularly true for high-resolution gratings that have specific resonance anomalies which were first observed by Wood [1] and subsequently subjected to extensive theoretical investigations [2]–[6]. These investigations have been expanded to resonance anomalies in a grating waveguide structure (GWS), and include new theoretical and experimental developments [7]–[16].

The basic GWS is comprised of a waveguide layer, a grating, and a substrate. The waveguide serves as a cavity in which discrete modes can propagate. A grating on top of the waveguide couples an incident illumination plane wave to the discrete modes within the waveguide. When the grating applies only a weak perturbation to the waveguide structure, the GWS will behave as a high-quality resonator with high finesse [14], [15].

A GWS can serve as a light modulator by dynamically varying its resonance wavelength [16]. Such dynamic variations are possible for GWS with high finesse, whereby they are highly sensitive to any dephasing process that changes the resonance condition. Accordingly, a shift of the resonance wavelength is achieved by modifying the refractive index in the waveguide or in adjacent layers of the GWS.

Manuscript received December 5, 2000; revised April 20, 2001.

N. Dudovich, G. Levy-Yurista, A. Sharon, and A. A. Friesem are with the Department of Physics of Complex Systems, The Weizmann Institute of Science, Rehovot 76100, Israel.

H.-G. Weber is with the Heinrich-Hertz-Institut für Nachrichtentechnik Berlin GmbH, Einsteinufer 37, 10587 Berlin, Germany.

Publisher Item Identifier S 0018-9197(01)05940-1.

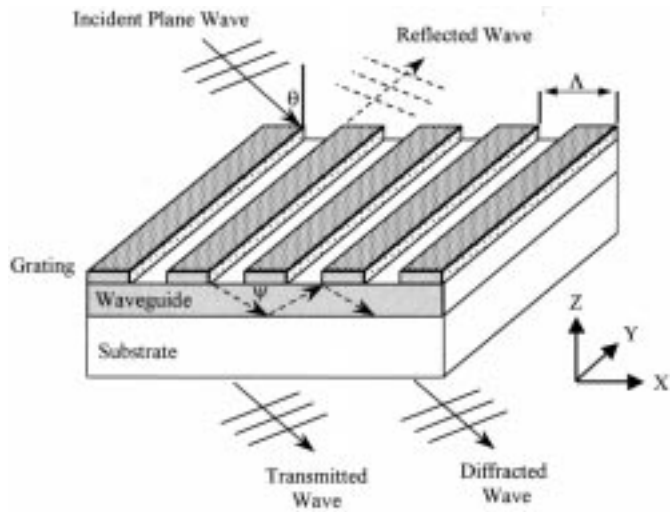


Fig. 1. Basic geometry of a grating-waveguide structure and relevant incident, transmitted, and diffracted waves. At resonance, there is destructive interference between the transmitted wave and the diffracted wave.

In this paper, we consider several existing theoretical models for changing the refractive index in semiconductor materials that can be applied to form an active GWS. The refractive index change is induced by applying an external electric field and by changing the free charge carrier density. By properly controlling material properties (e.g., the energy bandgap and doping concentration), as well as optical mode properties, the interaction between electrons and photons can be maximized. However, a large interaction induces high absorption in the waveguide cavity, which in turn reduces the finesse of the GWS, and accordingly determines a limit to the achievable resonance wavelength shift.

## II. Basic Principles of a GWS

In its most simple form, the GWS is comprised of a substrate, a waveguide layer, and a grating layer, as illustrated in Fig. 1. When such a structure is illuminated by an incident light beam, most of the beam is transmitted directly through the structure, while a small fraction is diffracted by the grating and trapped in the waveguide layer. Some of the trapped light in the waveguide layer is then rediffracted out, such that it interferes destructively with the transmitted part of the light beam. At a specific wavelength and angular orientation of the incident beam the structure resonates—namely, complete interference occurs and no light is transmitted. The basic relation between the resonant photon wavelength, the grating period and the propagating mode

0018–9197/01$10.00 © 2001 IEEE

wave-vector is derived by a momentum conservation equation to yield

$$n_{\mathrm{cl}} k \sin\theta + mK = n_{\mathrm{wg}} k \cos\psi \tag{1}$$

where

- $n_{\mathrm{cl}}$ refractive index of the cladding layer above the structure;
- $n_{\mathrm{wg}}$ refractive index of the waveguide layer;
- $\theta, \psi$ angle of the incident light and the angle of the diffracted light, respectively;
- $k$ $= 2\pi/\lambda_0$light wave-vector at resonance where $\lambda_0$ is the wavelength of the incident wave in vacuum;
- $K$ $= 2\pi/\Lambda$—grating wave-vector, where $\Lambda$ is the period of the grating;
- $m$ integer ($m = 1$ for the simplest case of a single-mode waveguide).

We utilized two different models for the analysis of the spectral behavior of a GWS [13]. The first is based on a geometrical ray picture approach for describing the multiple interference, similar to that used for analyzing the multiple interference in a Fabry–Perot resonator. According to this model, for a small diffraction coefficient the normalized transmission intensity ratio $T/T_0$ around the resonance ($T_0$ being the transmission off-resonance) can be approximated by a Lorentzian behavior, given by

$$\frac{T}{T_0} = \frac{\Delta k^2 + \alpha^2}{\Delta k^2 + (s+\alpha)^2} \tag{2}$$

where

- $\Delta k$ wave-vector detuning from the resonance wave-vector;
- $s$ coupling coefficient;
- $\alpha$ absorption coefficient.

The coupling coefficient $s$ depends on the thickness of the grating and waveguide layers, and on the refractive index of the different layers in the structure [13]. Proper design of the structure will lead to a certain coupling coefficient $s$, which determines the bandwidth of the transmission intensity. When $\alpha \ll s$, the absorption is negligible, and the transmission intensity ratio can approach zero at resonance. When $\alpha$ is of the order of $s$, the effect of absorption must be taken into account, whereby the transmission intensity ratio will be greater than zero at resonance, resulting in an increased resonance bandwidth. When $\alpha \gg s$, no resonance phenomena will be observed.

The second model for analyzing the resonance behavior of GWS is based on the coupled wave theory, in which Bragg coupling between two counter propagating modes is considered. The coupled wave model is an adaptation of a model used for analyzing DFB lasers that was developed by Kazarinov and Henry [17], and provides details on both the spectral bandwidth as well as the angular beamwidth of the GWS. It was shown that, according to this model, the spectral bandwidth and the angular beamwidth are not directly proportional to one another as in a Fabry-Perot resonator. According to (2), a reduced coupling coefficient will provide a narrow bandwidth. With current technology, the grating height and, thus, the coupling coefficient can be infinitely small, such that the bandwidth limit depends on unavoidable absorption. By controlling the different parameters of the GWS, the spectral resonance bandwidth can be designed to be of the order of 0.1 nm at the wavelength region of 1.55 $\mu$m [15] for which the achievable angular beamwidth can be considerably relaxed [13], which is of interest for spectral filtering and modulation applications.

## III. Refractive Index Change in Semiconductors

The resonance wavelength of the GWS can be controlled by varying the refractive index of the different layers in the structure. Such a variation of the refractive index leads to a different phase matching condition, and accordingly to a resonance wavelength shift. We considered several different effects that can lead to refractive index variations, which can be divided into two main subgroups: charge carrier-related effects and electric-field-related effects. Specifically, application of an external electric field and variations of the free charge carrier concentration will cause changes in the absorption coefficient of the waveguide which, in turn, induce changes in the refractive index via the Kramers-Kronig relation. Accordingly, changes in the absorption coefficient $\Delta\alpha$, within a wide range of the spectrum will induce changes in the refractive index $\Delta n$.

### A. Charge Carrier Effects

Charge carrier effects include primarily bandfilling and plasma effects, each dominant at different band gap energies of the semiconductor material [18]–[21].

*The bandfilling effect*, known also as the Burstein–Moss effect [18], is based on the decrease in absorption for photon energies near the nominal bandgap which results from an increase in carrier concentration. In a reverse bias configuration, the effect can be considered as band emptying where the carriers are removed from the depletion region and, as a result, the absorption edge shifts to lower energies.

Assuming parabolic bands, the absorption near the bandgap have a square-root law dependence in the photon energy. The change in the absorption coefficient is, therefore, calculated as [19], [20]

$$\Delta\alpha(N,P,E) = \sum_{\sigma} \frac{C_\sigma}{E} \sqrt{E - E_g} \{ f_v[E_{i\sigma}(P)] - f_c[E_{f\sigma}(N)] - 1 \} \tag{3}$$

where $N$ and $P$ are the free electrons and holes concentrations, respectively, and the sum is performed over the light-hole and the heavy-hole bands $\sigma$. $E = \hbar\omega$ is the photon energy, $E_g$ is the band gap energy, $C_\sigma$ is a constant defined by the appropriate matrix element, $f_v$ and $f_c$ are the Fermi–Dirac distribution functions for the valence band and the conduction band, respectively, and $E_{i\sigma}$ and $E_{f\sigma}$ are the initial and final states corresponding to band $\sigma$. The corresponding change in the refractive index is calculated through the Kramers–Kronig relation.

*The plasma effect* results from the free charge carrier absorption in either the conduction band or the valence bands. Using

the Drude model [21] the change in the refractive index can be calculated directly as

$$\Delta n(N,P) = \frac{-e^2\lambda_0^2}{8\pi^2 c^2 \varepsilon_0 n_0}\left(\frac{N}{m_e} + P\frac{m_{\rm hh}^{1/2}+m_{\rm lh}^{1/2}}{m_{\rm hh}^{3/2}+m_{\rm lh}^{3/2}}\right) \quad (4)$$

where

- $e$ electron charge;
- $c$ speed of light;
- $\varepsilon_0$ permittivity of the vacuum;
- $n_0$ unperturbed refractive index;
- $m_e$ effective mass of the electron;
- $m_{\rm hh}$ effective mass of the heavy hole;
- $m_{\rm lh}$ effective mass of the light hole.

### B. Electric-Field Effects

There are two main electric-field-related effects: the electrooptic effect characterized by a linear dependence of the change in the refractive index on the applied electric field, and the electrorefractive effect characterized by a quadratic dependence on the electric field.

*The electrooptic effect*, known also as the Pockels effect, is related to the biaxial birefringence induced by the presence of an electric field [22]. With InGaAsP semiconductor materials, the major axes of the index ellipsoid are rotated by 45° in the presence of the electric field $\mathbf{F}$. When the electric field is weak ($r_{41}F_z \ll n_0^{-2}$), the refractive indices along the new directions are

$$n_{x'} = n_0 - \frac{n_0^3}{2} r_{41} F_z \quad (5)$$

and

$$n_{y'} = n_0 + \frac{n_0^3}{2} r_{41} F_z \quad (6)$$

where $r_{41}$ is the nonzero element in the electrooptic tensor $r_{ij}$, and $(x', y')$ are the rotated major axes of the index ellipsoid. The refractive index change will have orientation dependence, being positive if the light propagates along the $[\bar{1}10]$ direction and negative if it propagates along the $[110]$ direction.

*The electrorefractive effect*, known also as the Franz–Keldysh effect, corresponds to the shift of the absorption edge to lower energies when an external electric field is applied [23]–[25]. The absorption coefficient can be calculated [24] as

$$\alpha(E,|\mathbf{F}|) = \sum_j A_j |\mathbf{F}|^{1/3}\left\{\left[\left.\frac{d\mathrm{Ai}(z)}{dz}\right|_{\beta_j}\right]^2 - \beta_j[\mathrm{Ai}(\beta_j)]^2\right\} \quad (7)$$

where

- $\beta_j$ $= B_j(E_g - E)|\mathbf{F}|^{-2/3}$;
- Ai Airy function;
- $A_j, B_j$ coefficients related to the parabolic band model in the limit when the field approaches zero.

The change in the refractive index is calculated using the Kramers–Kronig relation. For a low-intensity electric field, the change in the refractive index can be approximated as having a quadratic dependence on $|\mathbf{F}|$, given by

$$\Delta n = C(\lambda)|\mathbf{F}|^2 \quad (8)$$

where $C(\lambda)$ is a proportionality constant.

When applying an electric field across a junction, most of the particles move along the electric-field axis, therefore making the absorption and, accordingly, the electrorefractive effect polarization dependent. These polarization effects can be included by resorting to the theory of the polarization phenomena in electroabsorption [26], [27].

## IV. Design Considerations

In order to vary the refractive index in an active GWS by means of charge carriers and electric-field effects, several possible GWS configurations were considered. A basic property common to all configurations is that the free charge carrier concentration and the electric-field distribution can be controlled by the application of an external voltage.

The resonance shift $\Delta k$, due to a refractive index change $\Delta n$, can be derived approximately from (1). Assumption of a first-order approximation yields

$$\frac{\Delta k}{k} \approx \frac{\Delta n \cos\psi}{n_{\rm cl}\sin\theta + n_{\rm wg}\cos\psi}. \quad (9)$$

For the case of a small angle of incidence, (9) can be further approximated to give

$$\frac{\Delta k}{k} \approx \frac{\Delta n}{n_{\rm wg}}. \quad (10)$$

However, the maximal change of the refractive index applicable is limited by the maximal allowed absorption in accordance with the Kramers-Kronig relation. Accordingly, from (2) it is seen that the maximal tolerable absorption is limited by the required resonance bandwidth and maximal allowed attenuation of the transmission dip (the reflection peak), which are both loss-dependent.

Two types of active GWS configurations were considered: a forward-voltage configuration, in which charge carriers are injected into the waveguide region, and a reverse-voltage configuration, where charge carriers are depleted from the active region. Each configuration differs in its resonance tunability range, induced absorption, and response to the applied voltage.

In general, in the case of the forward-voltage configuration, the achievable tuning range can be relatively large, since high changes in charge carrier concentration can be induced. However, the injection of high levels of free charge-carriers concentrations require high current levels, since the area of the GWS is rather large (up to several mm$^2$). For example, we consider a typical case of a forward voltage configuration in a PIN structure with an area of 0.3 mm$^2$ and a resonance bandwidth of 1 nm. In that case, in order to achieve a tunability range of 4 nm, and a maximal allowed attenuation of the reflection peak to 75% of its original value, the required injection current is 3 A. In order to reduce the total current, the area of the GWS must be reduced accordingly. However, reducing the GWS area results in wider resonance bandwidths and greater sensitivity to alignment of the incident light beam.

In the case of reverse-voltage configurations, electric-field and carrier-related effects occur in the depletion region. In such structures, the depletion region width depends on the nature of the junction, the doping levels and the applied reverse voltage. In these configurations the achievable tuning range is usually

smaller compared to forward voltage configurations since the depletion region width decreases as the doping (and the free charge carriers concentration) increases. Therefore, the dependence of the refractive index change on the variation in charge carriers concentration is weaker in these configurations compared to the linear dependence induced in the forward voltage configurations. Furthermore, in the reverse voltage configurations, increasing the doping concentration will result in a lower breakdown voltage and, therefore, in a limited maximal change of the refractive index.

However, the main advantage of utilizing reverse voltage configurations is the ability to apply voltages rather than currents to the structure. Accordingly, the strict limitation over the GWS area imposed in forward-voltage configurations is relaxed considerably. This enables the design and utilization of narrower resonance bandwidths that can be of the order of several tenths of a nanometer in the wavelength region of 1.55 $\mu$m.

Here, we chose to concentrate on high-finesse GWSs with narrow resonance bandwidths. In such structures, the tolerable absorption is relatively small, leading to a limited tunability range. Therefore, following the above discussion, we chose to consider a reverse-voltage configuration.

In order to evaluate the effective refractive index change for a given active GWS configuration, we calculated the interaction of the optical mode and the active region. Using Poisson's equation and taking into account the continuity of the field and the potential at the interface between the different layers, the depletion width and the electric-field distribution can be calculated [28]. The effect of the interaction between the optical mode and the refractive index change $\Delta n$ in the depletion region is defined as the effective refractive index change $\Delta n_{\text{eff}}$

$$\Delta n_{\text{eff}} \equiv \frac{1}{N_c}\left(\int_{-X_p(V)}^{X_n(V)} \Delta n(V,x) I(x)\,dx - \int_{-X_p(0)}^{X_n(0)} \Delta n(0,x) I(x)\,dx\right) \tag{11}$$

where

$V$ applied voltage;

$X_n$, $X_p$ depletion region edges at the $n$- and $p$-doped regions, respectively;

$I(x)$ mode intensity profile;

$N_c$ normalization constant.

This evaluation is a first-order approximation, valid for $\Delta n \ll n_0$. Carrier-related effects are assumed to be constant in the depletion region. Accordingly, the resulting $\Delta n_{\text{eff, carriers}}$ is given by

$$\begin{aligned}\Delta n_{\text{eff,carriers}} &= \Delta n_{\text{carriers}} \frac{1}{N_c}\left(\int_{-X_p(V)}^{X_n(V)} I(x)\,dx - \int_{-X_p(0)}^{X_n(0)} I(x)\,dx\right)\\ &= \Delta n_{\text{carriers}}(\Gamma_V - \Gamma_0)\end{aligned} \tag{12}$$

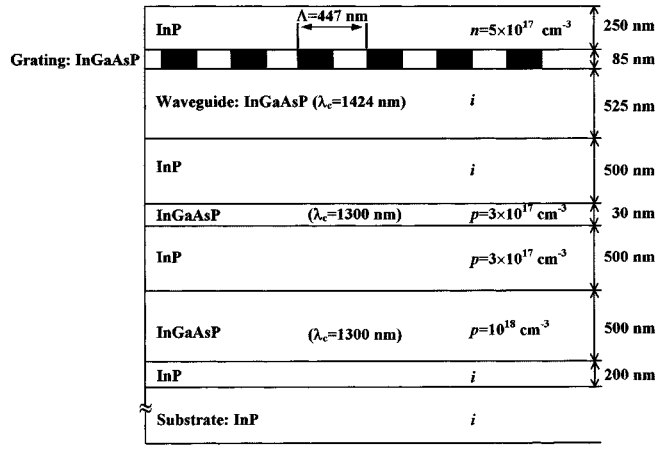


Fig. 2. Schematic configuration of the layer structure of an active GWS designed to operate with reverse voltages.

where $\Delta n_{\text{carriers}}$ is the refractive index change corresponding to carrier-related effects, and $\Gamma_V$ is the modal filling factor, defined by

$$\Gamma_V \equiv \frac{1}{N_c}\int_{-X_p(V)}^{X_n(V)} I(x)\,dx. \tag{13}$$

The tunability range of an active GWS based on a reverse-voltage configuration depends mainly on the bandgap wavelength of the GWS materials, the doping concentration of the different layers, and the junction's location with respect to the optical mode. Maximizing the effective refractive index change can be achieved by exploiting effects such as the bandfilling and electrorefractive effects. These effects are dominant where the incident light wavelength is close to the bandgap wavelength of the waveguide material. Furthermore, a proper design of the different layers doping concentration and the location of the junction with respect to the waveguide result in a large modal filling factor. However, the doping levels are limited by the maximal allowed absorption. Consequently, the tunability range of an active GWS can be maximized.

## V. Fabrication of Active GWS

Following the considerations discussed above, we fabricated several active GWS samples based on a reverse-voltage configuration. The configuration of a representative active GWS sample is illustrated in Fig. 2. The substrate is an intrinsic InP layer, on top of which an additional intrinsic InP layer was grown with MOCVD. The next layer is a highly $p$-doped $10^{18}$ cm$^{-3}$ InGaAsP layer, followed by $3 \times 10^{17}$cm$^{-3}$ $p$-doped InP and InGaAsP layers, an intrinsic InP layer, and an intrinsic InGaAsP layer with bandgap wavelength $\lambda_c$ of 1424 nm that serves as the waveguide layer and the grating layer. The grating was formed by first using an electron beam to record the grating on a AZPN114 photo-resist, which was developed to form a grating mask, and then etched into the InGaAsP layer with a selective ion-etching process. After removing the photo-resist residuals, a final grating of 85-nm thickness with a 50% duty cycle and waveguide of 525-nm thickness were formed. A $5 \times 10^{17}$cm$^{-3}$ $n$-doped layer of InP was added above the

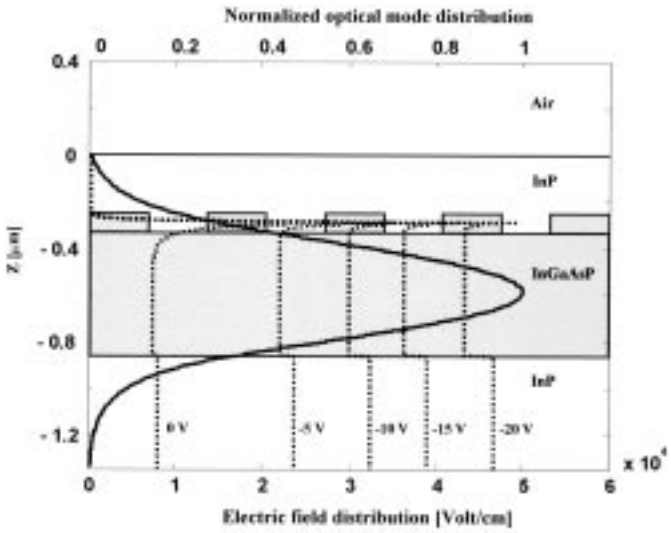


Fig. 3. Calculated normalized optical mode distribution (solid curve) with respect to the different layers of the GWS of Fig. 2, and several electric-field distributions (dotted curves) induced by the application of different voltage levels of $0, -5, -10, -15,$ and $-20$ V. These voltage levels include an unavoidable voltage drop across the imperfect contacts of this specific sample.

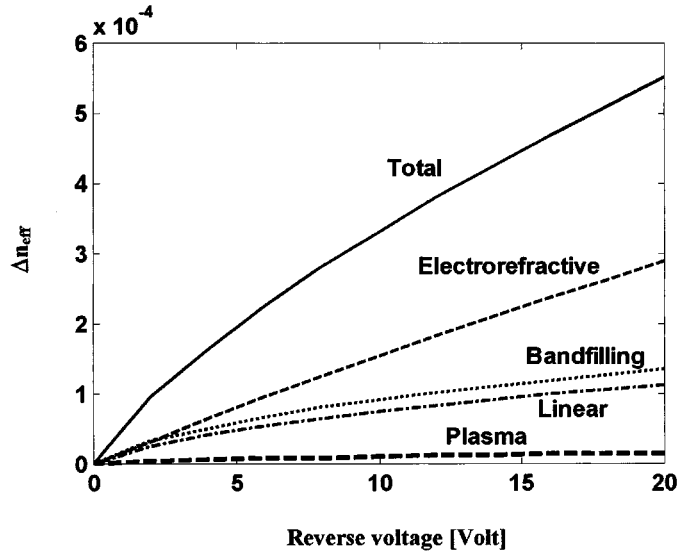


Fig. 4. Calculated change of the effective refractive index for the different effects as a function of the reverse voltage for the GWS configuration of Fig. 2, for TE polarization and illumination wavelength of 1580 nm.

grating with MOCVD. The thicknesses of the various layers are given in Fig. 2.

Since the difference between the refractive index of the waveguide layer and that of the cladding layer is relatively high, the optical mode is well confined. In addition, the amplitude of the grating perturbation is high, resulting in a relatively large coupling constant.

The $pn$ junction is located at the upper interface of the waveguide. Since the doping in the $n$ region is a few orders of magnitude higher than the nonintentionally doped waveguide, the width of the depletion region in the $n$ region is considerably smaller than the width of the waveguide layer. In this configuration, the depletion region penetrates through the waveguide layer into the intrinsic InP layer. As a result, a large overlap between the active region and the optical mode is achieved. However, since the waveguide is nonintentionally doped, the changes induced by the external voltage are limited compared to a higher doped waveguide layer. Moreover, since the bandgap wavelength $\lambda_c$ in the waveguide is relatively close to the illumination wavelength $\lambda_0$ ranging from 1490 to 1590 nm, and the doping of the waveguide is particularly low, carrier-related effects are relatively small, and the electrorefractive effect is dominant.

Fig. 3 shows the calculated normalized optical-mode distribution (solid curve) with respect to the different layers of the active GWS shown in Fig. 2, and several electric-field distributions (dotted curves) induced by the application of different reverse-voltage levels. These voltage levels include an unavoidable voltage drop across the imperfect contacts of this specific sample. It is seen that increasing the applied reverse voltage results in an enhancement of the electric-field amplitude in the waveguide. Accordingly, a larger effective refractive index change $\Delta n_{\text{eff}}$ is induced, leading to an increased resonance wavelength shift.

Fig. 4 shows the calculated change of the effective refractive index as a function of reverse voltage for TE polarization and for illumination wavelength of 1580 nm, according to (11) and (12). Since the depletion region penetrates into the non-intentionally doped InP layer, the overlap $\Gamma$ between the optical mode and the active region is almost constant as a function of the voltage. The change of the effective refractive index due to the linear electrooptic effect $\Delta n_{\text{eff,leo}}$ varies with the voltage as $\sqrt{|V|}$, since $\Delta n_{\text{eff,leo}} \propto |\mathbf{F}| \cdot \Gamma \propto |\mathbf{F}|$, and $|\mathbf{F}| \propto |V|/X_p \propto \sqrt{|V|}$.

The change of the effective refractive index due to the electrorefractive effect $\Delta n_{\text{eff,er}}$, is almost linear with the voltage, since $\Delta n_{\text{eff,er}} \propto |\mathbf{F}|^2 \cdot \Gamma \propto |\mathbf{F}|^2 \propto |V|$. The change of the effective refractive index due to the bandfilling effect $\Delta n_{\text{eff,bf}}$ varies with the voltage as $\sqrt{|V|}$, since the active region for this effect is dominated by $X_n, \Delta n_{\text{eff,bf}} \propto X_n \propto \sqrt{|V|}$, and the plasma effect is negligible. It should be mentioned that although $X_n$ is relatively narrow, the bandfilling effect is rather large such that the effective refractive index change induced by it is not negligible.

The change of the effective refractive index also depends on the polarization of the illumination. For the TM polarization, the linear electrooptic effect is not induced by the external voltage. Thus, at low reverse-voltage levels for which the linear electrooptic effect is relatively large, the change of the refractive index for the TE polarization is greater than that for the TM polarization. The electrorefractive effect depends on polarization but in a more complex manner,[1] and is larger for the TM polarization. Accordingly, at high reverse voltage levels, the change in the refractive index is greater for the TM case.

Following the above calculations, it was found that the absorption is dominated by electroabsorption and is, therefore, highly sensitive to the illumination wavelength and polarization.

[1]In order to evaluate this dependency we approximated the inequality relation (5) in [26] as a step function.

## VI. Experimental Procedure and Results

The experimental arrangement that was used for evaluating the active GWS samples is illustrated in Fig. 5. It included a tunable external cavity diode laser operating in the wavelength range of 1490–1590 nm with a spectral resolution better than 3 pm. The beam from the laser was coupled to a single mode fiber and then expanded, collimated and polarized to obtain a linearly polarized plane wave. Part of the plane wave was directed toward the GWS, which was placed on a translating/rotating stage. The light reflected from the GWS was collected by detector $D_1$ and the other part of the beam was collected by detector $D_2$ for normalization. We applied reverse voltages to the GWS sample using a voltage source with a high-accuracy current limit, which allowed achievement of the maximum voltage possible before reaching the breakdown voltage. A computer was used for controlling the laser, the translating/rotating stage, the detectors and the voltage source. A HeNe laser beam, transmitted through a beam combiner to be collinear with the tunable diode laser beam, served to align the GWS samples with the incident beam.

Using the experimental setup illustrated in Fig. 5, we measured several properties of the active GWS samples, the results of which are presented in Figs. 6–8. Fig. 6 shows the calculated and measured resonance wavelength shift as a function of the applied reverse voltage. The resonance shift for two different representative resonance wavelengths was first calculated and then measured for both the TE and TM polarizations. The choice of these resonance wavelengths, limited by the tunability range of the laser, allowed for the characterization of the refractive index change effects at different spectral regions with respect to the bandgap wavelength, $\lambda_c$. The calculated results were obtained by numerical procedure following (11) and (12). The measured resonance wavelengths were set by choosing the angular orientation of the incidence beam so as to induce two different counter propagating modes in the waveguide, each of which has a different resonance wavelength [13]. In our experiments, these initial resonance wavelengths were about 1520 and 1586 nm for TE polarization, and 1515 and 1580 nm for TM polarization, all set at an incidence angle of 4.3°. Fig. 6(a) shows the calculated and measured resonance wavelength shift for the case of TE polarization. The measured resonance wavelength shift increased for the shorter wavelength which was closer the bandgap wavelength, $\lambda_c = 1424$ nm. A maximal resonance wavelength shift of 0.44 nm was measured at a reverse voltage of $-24.5$ V at a resonance wavelength of 1520 nm, whereas a lower resonance wavelength shift of 0.33 nm was measured at a similar voltage at a resonance wavelength of 1586 nm. Fig. 6(b) shows the resonance wavelength shift for the case of TM polarization. The maximal resonance wavelength shift measured was 0.68 nm at a reverse voltage of $-24.5$ V at a resonance wavelength of 1515 nm, and a wavelength shift of 0.43 nm at a reverse voltage of $-29$ V at the resonance wavelength of 1580 nm. Accordingly, we deduce that for both the TE and the TM polarizations, the resonance wavelength shift as a function of the reverse voltage was larger for the shorter resonance wavelengths which are closer to the bandgap wavelength, $\lambda_c$. At high reverse-voltage levels, the resonance wavelength shift for the TM polarization is larger than for the TE polarization, since in this voltage region the effective refractive index change is dominated by the electrorefractive effect which is higher for the TM case. It is evident that the measured and calculated results are in good agreement.

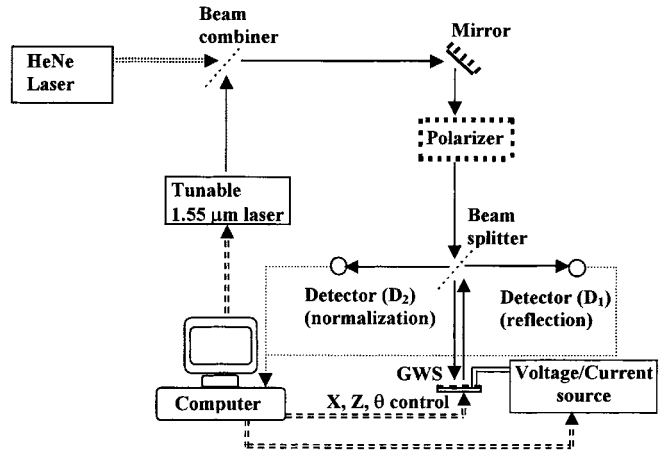


Fig. 5. Experimental arrangement to evaluate the active GWS.

Fig. 7 shows the calculated and the measured absorption coefficient as a function of the reverse voltage for TE and TM polarizations, each with the same two resonance wavelengths used in Fig. 6. The measured absorption coefficient results were obtained indirectly from the measurements of the attenuation of the reflected intensity peak at resonance and the broadening of resonance bandwidth, both as a function of the reverse voltage. The resonance shape was approximated by a Lorentzian function according to (2).

Fig. 7(a) shows the calculated and measured absorption coefficient as a function of the applied reverse voltage for the case of TE polarization. It is seen that increasing the applied reverse voltage resulted in a larger measured absorption coefficient. Moreover, as the resonance wavelength approached the bandgap wavelength $\lambda_c$, the absorption coefficient curve became steeper. Accordingly, for a reverse voltage of $-25$ V we measured an absorption coefficient of 6.9 cm$^{-1}$ at the resonance wavelength of 1520 nm, whereas at the resonance wavelength of 1586 nm, we measured an absorption coefficient of only 1.25 cm$^{-1}$. Fig. 7(b) shows the calculated and measured absorption coefficient as a function of the reverse voltage for the case of TM polarization. As in the TE case, the absorption coefficient increased as the wavelength approached the bandgap wavelength $\lambda_c$. In this case, the measured absorption coefficient was 11.7 cm$^{-1}$ at the resonance wavelength of 1515 nm and at a reverse voltage of $(-18)$ V. At the resonance wavelength of 1580 nm, we measured an absorption coefficient of only 5.5 cm$^{-1}$ at the maximal applicable reverse voltage of $(-29)$ V. As is evident, the absorption is highly sensitive to the resonance wavelength and the polarization, increasing dramatically as the resonance wavelength approached the bandgap wavelength $\lambda_c$. When the absorption coefficient increased considerably above the resonance bandwidth ($\Delta k = 13$ cm$^{-1}$), the contrast ratio was very low and the resonance bandwidth very large, such that tunability

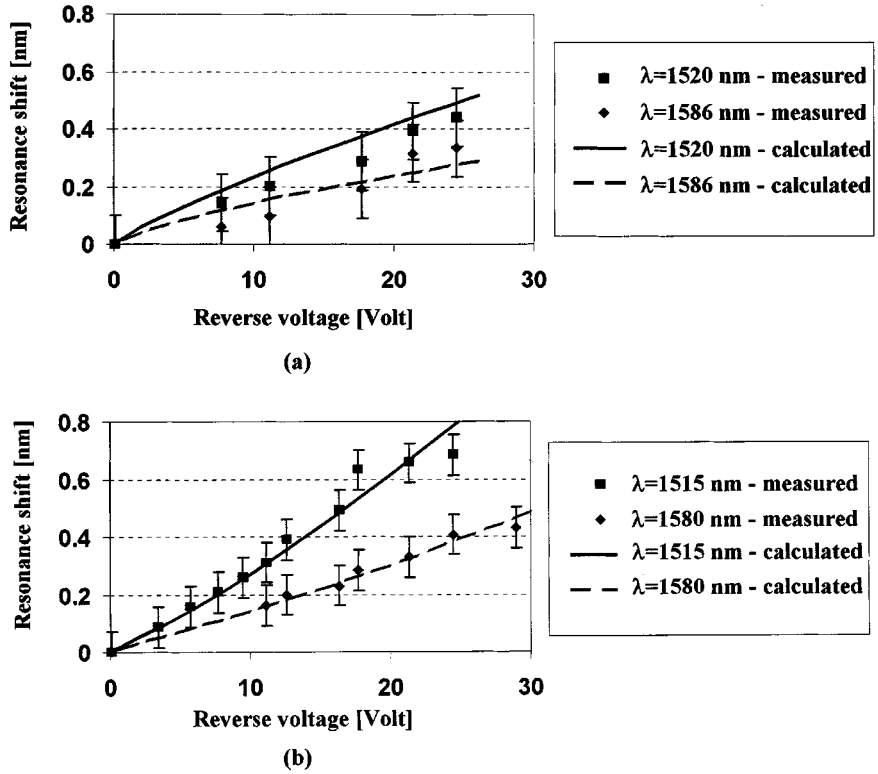


Fig. 6. Calculated and measured resonance wavelength shift as a function of the applied reverse voltage for two different resonance wavelengths. (a) TE polarization. (b) TM polarization.

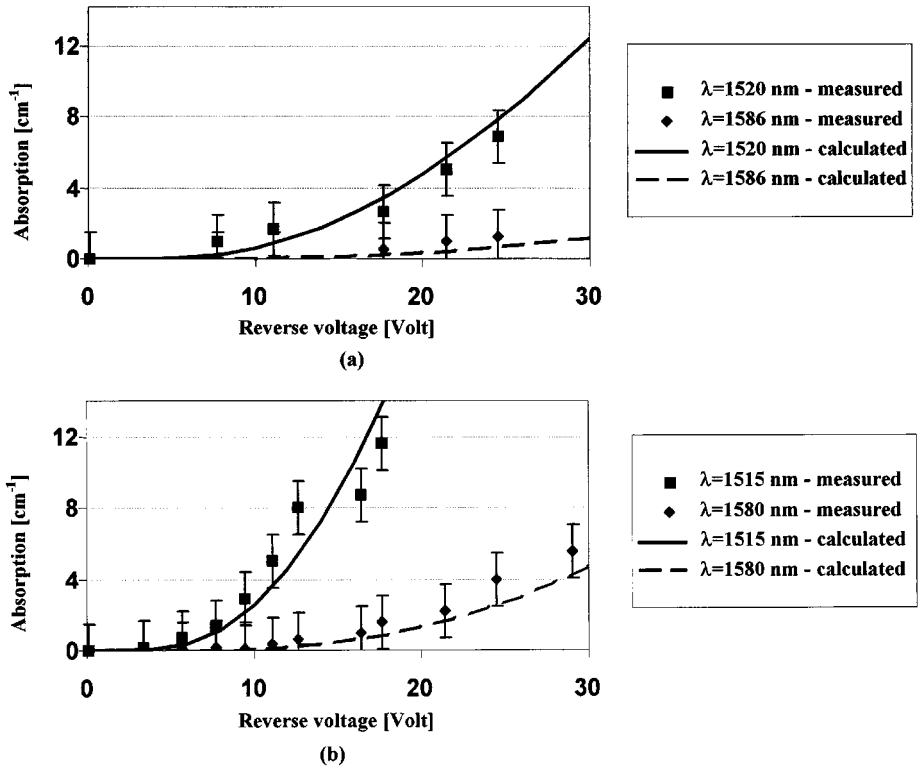


Fig. 7. Calculated and measured absorption coefficient as a function of the reverse voltage for two different resonance wavelengths. (a) TE polarization. (b) TM polarization.

became impractical. The dependence of the measured absorption coefficient on the resonance wavelength and polarization is compatible with the numerical calculations.

Using a constant reverse voltage and changing the incidence beam orientation angle from 0° to 4.5°, we measured the dependence of the wavelength shift on the initial resonance wave-

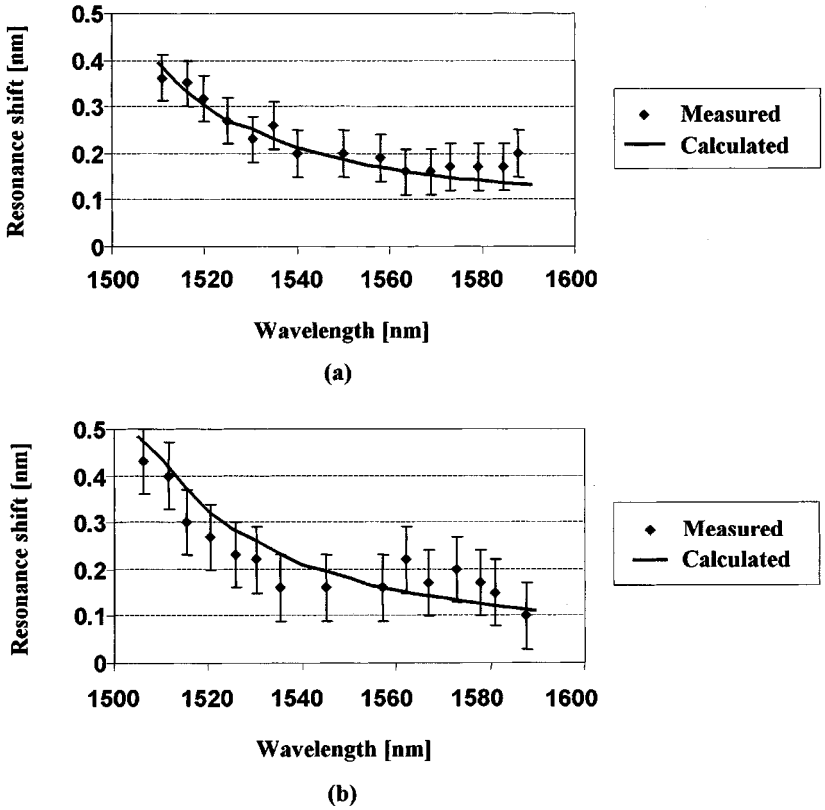


Fig. 8. Calculated and measured resonance shift as a function of the resonance wavelength for a constant reverse voltage of $-12$ V. (a) TE polarization. (b) TM polarization.

length. Fig. 8 shows the calculated and the measured resonance wavelength shift for a constant reverse voltage of $-12$ V as a function of the resonance wavelength for TE and TM polarizations. The choice of the relatively low reverse voltage of $-12$ V allowed measurements even at wavelengths rather close to $\lambda_c$, where the electrorefractive absorption was considerably high.

Fig. 8(a) shows the calculated and measured resonance wavelength shift for the case of TE polarization. It is seen that, as the resonance wavelength approached the bandgap wavelength, $\lambda_c$, the measured resonance wavelength shift increased. Specifically, an increase of 80% in the resonance wavelength shift was measured, from a wavelength shift of 0.2 nm at the resonance wavelength of 1588 nm to a wavelength shift of 0.36 nm at the resonance wavelength of 1511 nm. Fig. 8(b) shows the calculated and measured resonance wavelength shift for the case of TM polarization. The effect in this case was more substantial than in the TE polarization. Specifically, an increase of over 300% in the wavelength shift is measured, from a wavelength shift of 0.1 nm at the resonance wavelength of 1588 nm to a wavelength shift of 0.43 nm at the resonance wavelength of 1506 nm. As is evident, good agreement between the measured and the calculated resonance wavelength shift was obtained. At a reverse voltage of $-12$ V, the linear electrooptic effect is not negligible compared to the electrorefractive effect. As a result, in the long wavelengths region, the resonance wavelength shift was higher for TE polarization than for TM polarization. As the wavelength decreased the electroabsorption effect increased, resulting in a larger wavelength shift for the TM polarization.

In summary, we established that as the resonance wavelength is closer to the bandgap wavelength $\lambda_c$, both the resonance wavelength shift and the absorption coefficient increase. We also established that the resonance shift and the absorption coefficient are larger for TM polarization than for TE polarization. Good agreement between the numerical calculations and the measurements was obtained. The maximum resonance wavelength shift of 0.68 nm was achieved for TM polarization at a resonance wavelength of 1515 nm and a reverse voltage of $-24.5$ V. The reflected intensity at the maximum wavelength shift was 20% lower than the reflected intensity at the initial resonance wavelength. At the shorter wavelengths, the maximal resonance shift was limited by absorption. At the longer wavelengths where absorption is reduced, the resonance wavelength shift was limited by the breakdown voltage.

## VII. Concluding Remarks

Interest in resonant phenomena in gratings has long been reported. The fabrication of such structures became feasible with the advent of sub-micron photolithography and planar processing technology, where the dimensions are of the order of the wavelength of light and smaller. Such structures of this size scale can be used to manipulate the phase of the light, to give an interference effect with a spectral bandwidth and angular beamwidth that can be tailored for specific applications. Utilizing advanced techniques such as MOCVD or MBE enabled researchers meeting the high accuracy demands required in fabrication of practical devices.

In this paper, we presented an active GWS in which semiconductor materials are incorporated. We considered several effects which induce refractive index changes, both by adapting theoretical analytical models and by resorting to numerical calculations. These effects include the bandfilling effect, the plasma effect, the electrooptic effect, the electrorefractive effect, and some combination of them. Accordingly, we investigated the resonance wavelength shift, the reduction in reflected intensity, and the resonance bandwidth-broadening resulting from these effects. Following these investigations, we considered the active GWS dependence on the semiconductor bandgap wavelength, the illumination wavelength, the free-charge carrier concentration, and the application of an external electric field. Furthermore, we considered the dependence on the geometrical and optical parameters of the structure. The outcome of these investigations was utilized for the design and fabrication of active GWS's with InGaAsP/InP materials based on a reverse-voltage configuration.

Following the fabrication of these active GWSs, we conducted several experimental procedures to support our theoretical predictions and calculations. Specifically, we measured the resonance wavelength shift of an active GWS, as well as the induced absorption as a function of the external voltage, the resonance wavelength, and the incident light polarization. Good agreement between measured and calculated results was obtained.

Finally, we indicate that our theoretical and experimental results suggest that applications such as dynamic narrow-band spectral filters, optical switches, and spatial light modulators may be feasible. Such devices should be useful in advanced signal processing, WDM applications and communications systems. Moreover, since the GWS is inherently planar and can be made to operate with small refractive index changes, it is interesting to contemplate the further possibility of incorporating active GWS modulators directly on semiconductor chips for the optical interconnection of processors.

## ACKNOWLEDGMENT

The authors acknowledge helpful discussions with Dr. D. Rosenblatt, as well as the support, in part, of the Israeli Ministry of Science and the Bundesministerium for Forschung and Technologie.

## REFERENCES

[1] R. W. Wood, "On a remarkable case of uneven distribution of light in a diffraction grating spectrum," *Philos. Mag.*, vol. 4, pp. 396–402, 1902.

[2] A. Hessel and A. A. Oliner, "A new theory of Wood's anomalies," *Appl. Opt.*, vol. 4, pp. 1275–1297, 1965.

[3] M. Neviere, *Electromagnetic Theory of Gratings*, R. Petit, Ed. Berlin, Germany: Springer-Verlag, 1980, ch. 5.

[4] S. T. Peng and T. Tamir, "Theory of periodic dielectric waveguides," *IEEE Trans. Microwave Theory Tech.*, vol. MTT-23, pp. 123–133, 1975.

[5] G. A. Golubenko, A. S. Svakhin, V. A. Sychugov, and A. V. Tischenko, "Total reflection of light from a corrugated surface of a dielectric waveguide," *Sov. J. Quantum. Electron.*, vol. 15, pp. 886–887, 1985.

[6] E. Popov, L. Mashev, and D. Maystre, "Theoretical study of anomalies of coated dielectric gratings," *Opt. Acta*, vol. 32, pp. 607–629, 1986.

[7] I. A. Avrutskii, G. A. Golubenko, V. A. Sychugov, and A. V. Tischenko, "Light reflection from the surface of a corrugated waveguide," *Sov. Tech. Phys. Lett.*, vol. 11, pp. 401–402, 1985.

[8] I. A. Avrutskii and V. A. Sychugov, "Reflection of a bounded light beam from the surface of periodically perturbed waveguide," *Sov. Tech. Phys. Lett.*, vol. 32, pp. 235–237, 1987.

[9] R. Magnusson and S. S. Wang, "Optical grating-waveguide filters," *SPIE*, vol. 2108, pp. 380–391, 1993.

[10] S. S. Wang and R. Magnusson, "Theory and applications of guided-mode resonance filters," *Appl. Opt.*, vol. 32, pp. 2606–2613, 1993.

[11] S. Peng and G. M. Morris, "Experimental demonstration of resonant anomalies in diffraction from two dimensional gratings," *Opt. Lett.*, vol. 21, pp. 549–551, 1996.

[12] S. Tibuleac and R. Magnusson, "Diffractive narrow-band transmission filters based on guided-mode resonance effects in thin-film multilayers," *IEEE Photon. Technol. Lett.*, vol. 9, pp. 464–466, 1997.

[13] D. Rosenblatt, A. Sharon, and A. A. Friesem, "Resonant grating waveguide structures," *IEEE J. Quantum Electron.*, vol. 33, pp. 2038–2059, 1997.

[14] A. Sharon, A. A. Friesem, and D. Rosenblatt, "Narrow spectral bandwidths with grating-waveguide structures," *Appl. Phys. Lett.*, vol. 69, pp. 4154–4156, 1997.

[15] G. Levy-Yurista and A. A. Friesem, "Very narrow spectral filters with multilayered grating-waveguide structures," *Appl. Phys. Lett.*, vol. 77, pp. 1596–1598, 2000.

[16] A. Sharon, D. Rosenblatt, A. A. Frisem, H. G. Weber, H. Engle, and R. Steingrueber, "Light modulation with resonance grating-waveguide structures," *Opt. Lett.*, vol. 21, pp. 1564–1566, 1996.

[17] R. Kazarinov and C. Henry, "Observation of destructive interference in the radiation loss of second-order distributed feedback lasers," *IEEE J. Quantum Electron.*, vol. 21, pp. 151–153, 1985.

[18] E. Burstein, "Anomalous optical absorption limit in InSb," *Phys. Rev.*, vol. 93, pp. 632–633, 1954.

[19] N. G. Nilsson, "Empirical approximations for Fermi energy in a semiconductor with parabolic bands," *Appl. Phys. Lett.*, vol. 33, pp. 653–654, 1978.

[20] B. R. Bennett, R. A. Soref, and J. A. del Alamo, "Carrier-induced change in refractive index of InP, GaAs, and InGaAsP," *IEEE J. Quantum Electron.*, vol. 26, pp. 113–122, 1990.

[21] N. W. Ashcroft and N. D. Mermin, *Solid State Physics*. Philadelphia, PA: HRW, 1976, ch. 1.

[22] A. Yariv, *Optical Electronics*, 4th ed. Philadelphia, PA: HRW, 1991, pp. 309–316.

[23] J. Callaway, "Optical absorption in an electric field," *Phys. Rev.*, vol. 130, pp. 549–553, 1963.

[24] K. Tharmalingham, "Optical absorption in the present of a uniform field," *Phys. Rev.*, vol. 130, pp. 2204–2206, 1963.

[25] D. E. Aspnes, "Electric field effects on the dielectric constant of solids," *Phys. Rev.*, vol. 153, pp. 972–982, 1967.

[26] L. V. Keldysh, O. V. Konstantinov, and V. I. Perel, "Polarization effect in the interband absorption of light in semiconductors subjected to a strong electric field," *Sov. J. Phys. Semicond.*, vol. 3, pp. 876–884, 1970.

[27] N. K. Dutta and N. A. Olsson, "Electroabsorption in InGaAsP-InP double heterostructures," *Electron. Lett.*, vol. 20, pp. 634–635, 1984.

[28] N. W. Ashcroft and N. D. Mermin, *Solid State Physics*. Philadelphia, PA: HRW, 1976, ch. 29.

**Nirit Dudovich** was born in Jerusalem, Israel, on in 1971. She received the B.Sc. degree in physics and computer science from Tel Aviv University, Tel Aviv, Israel, and the M.Sc. degree in applied physics from Weizmann Institute of Science, Rehovot, Israel, where she is currently working toward the Ph.D. degree in the Department of Physics of Complex Systems.

Her research has included resonant-grating waveguide structures based on semiconductor materials, ans more recently includes quantum coherent control with femtosecond pulses.

**Guy Levy-Yurista** was born in Tel Aviv, Israel, in 1969. He received the B.Sc. degree in physics and mathematics from the Hebrew University, Jerusalem, Israel, in 1990 and the M.Sc. degree in applied physics from Tel Aviv University, Tel Aviv, Israel, in 1996. He is currently completing the Ph.D. degree in physics at the Department of Physics of Complex Systems, Weizmann Institute of Science, Rehovot, Israel.

From 1990 to 1995, he was part of a research group at the Government Research Laboratories, Tel Aviv, Israel. His research field was near- and far-infrared applied physics. At Tel Aviv University, he was involved in a research of chaotic effects in tapered laser structures. At Weizmann Institute of Science, he conducted research in passive and active resonant-grating waveguide structures based on semiconductor, polymer and liquid-crystal based materials.

Mr. Levy-Yurista is the Chief Associate Editor of the *Israeli Wine Magazine*, lecturing on different aspects of the wine world in Tel Aviv.

**Avner Sharon**, photograph and biography not available at the time of publication.

**Asher A. Friesem** (S'57–M'62–SM'79–F'95) received the B.Sc. and Ph.D. degrees from the University of Michigan, Ann Arbor, in 1958 and 1968, respectively.

From 1958 to 1963, he was with Bell Aero Systems Company, Buffalo, NY, and Bendix Research Laboratories, Southfield, MI. From 1963 to 1969, he was with the University of Michigan Institute of Science and Technology, conducting investigations in coherent optics, mainly in the areas of optical data processing and holography. From 1969 to 1973, he was the Principal Research Engineer in the Electro-optics Center of Harris, Inc., Ann Arbor, MI, performing research in the areas of optical memories and displays. In 1973, he joined the staff of the Weizmann Institute of Science, Rehovot, Israel, becoming a Professor of Optical Sciences in 1977. He is concerned with new holographic concepts and applications, optical image processing, and electrooptics devices.

Dr. Friesem is the Vice President of the International Commission of Optics and Chairman of the Israel Laser and Electro-Optics Society. He is a Fellow of the Optical Society of America, and a member of SPIE, Eta Kappa Nu, and Sigma Xi.

**Hans-Georg Weber**, photograph and biography not available at the time of publication.